00FCC-27

Speed-Sensorless Control of Induction Motors for Electric Vehicles

Fang Z. Peng and Donald J. Adams
Oak Ridge National Laboratory♠

Copyright © 1999 Society of Automotive Engineers, Inc.

ABSTRACT

An electric bus system has been operating in the downtown area of Chattanooga, Tennessee for more than four years. The buses use traditional hard-switched IGBT inverters driving special induction motors with a speed sensor (tachometer) and two embedded flux-sensing windings to provide rotor speed and flux information to the motor controller for implementation of high performance field oriented control (vector control). The induction motor is oil-cooled and equipped with an internal planar gear reduction. The current system has experienced failures in both speed sensors and flux sensors because they are unreliable, susceptible to EMI and must operate in a hostile environment created by oil leaks. A speed- and flux-sensorless induction motor drive system with a new 100 kW soft-switching inverter has been implemented to replace the existing system. The new soft-switching inverter is able to provide 300 A (rms) and 230 V (rms) continuous power to the motor with no voltage surges and reduced dv/dt (<300V/us) at switching. The new inverter also draws ripple-less DC current from the battery. As a result, the new inverter is friendly to the motor and battery. Extended lifetime is expected for both the motor and battery. The new inverter with the speed- and flux-sensorless control has been road-tested and has achieved satisfactory performance. The project was supported under the Department of Energy (DOE) funding and local industry partnership.

INTRODUCTION

For electric vehicle traction drive applications, it is always desirable to implement a speed sensorless control in terms of cost reduction and reliability improvement. However, a speed-sensorless motor control system usually has poor dynamic performance and performance deterioration with temperature-change related parameter variations.

The familiar difficult problems with traditional speed- and flux-sensorless control include: (1) the speed self-sensing at starting and low speed region becomes unstable and (2) without accurate speed information, torque control becomes difficult, resulting in a lack of starting torque and jerky-start situation. This is because most traditional methods of speed identification are based on the flux model requiring pure integral calculation of sensed current and voltage [1, 2]. The pure integral calculation becomes impossible at low and zero speeds in the circuitry and the algorithm causes DC drift and inaccuracy. Many improvements have been made to overcome this integration problem [3, 7].

The new speed self-sensing method developed is based on the back electromotive force (EMF) model of the induction motor, which can alleviate the above problems. The new speed- and flux-sensorless vector control has been implemented with a 100 kW soft-switching inverter specially developed to drive the bus and has been extensively road-tested. The test results have demonstrated the new system's feasibility, smooth start,

♠ Prepared by the Oak Ridge National Laboratory, Oak Ridge, managed by Lockheed Martin Energy Research Corp. for the U. S. Department of Energy under contract DE-AC05-96OR22464.

The submitted manuscript has been authored by a contractor of the U. S. Government under contract No. DE-AC05-96OR22464. Accordingly, the U. S. Government retains a nonexclusive, royalty-free license to publish or reproduce the published form of this contribution, or allow others to do so, for U. S. Government purposes.

and good torque control at low speeds. As a result, the implementation of the new speed- and flux-sensorless control improves reliability, reduces costs, and makes it possible to use commercially available induction motors. This paper presents the speed identification method and reports the test results.

SPEED IDENTIFICATION PRINCIPLE

The *dq* equations of an induction motor are expressed as

$$\boldsymbol{v_s} = R_s \boldsymbol{i_s} + \sigma L_s \frac{d\boldsymbol{i_s}}{dt} + \boldsymbol{e_m}\,, \tag{1}$$

$$\frac{d\boldsymbol{i_m}}{dt} = \boldsymbol{\omega_r} \otimes \boldsymbol{i_m} - \frac{1}{T_r}\boldsymbol{i_m} + \frac{1}{T_r}\boldsymbol{i_s}\,, \tag{2}$$

where

$\boldsymbol{v_s} = [v_{sd}\,,\ v_{sq}]^T$ is the stator voltage vector,

$\boldsymbol{i_s} = [i_{sd}\,,\ i_{sq}]^T$ is the stator current vector,

$\boldsymbol{i_r} = [i_{rd}\,,\ i_{rq}]^T$ is the rotor current vector,

$\boldsymbol{i_m} = \boldsymbol{i_s} + (L_r/L_m)\boldsymbol{i_r}$ is the magnetizing current vector,

$\boldsymbol{e_m} = L'_m d\boldsymbol{i_m}/dt$ is the back EMF vector,

L_s, L_r, and L_m are the stator, rotor, and mutual inductance, respectively,

$\sigma = 1 - L_m^2/(L_s L_r)$ is the leakage coefficient,

$L'_m = L_m^2 / L_r$ is the equivalent mutual inductance,

R_s and R_r are the stator and rotor resistance, respectively,

$T_r = L_r / R_r$ is the rotor circuit time constant,

$\boldsymbol{\omega_r}$ is the rotor speed vector, and $\otimes$ denotes the vector product.

From (1) and (2), the back EMF vector, $\boldsymbol{e_m}$, can be derived as follows:

$$\boldsymbol{e_m} = \boldsymbol{v_s} - \left(R_s \boldsymbol{i_s} + \sigma L_s \frac{d\boldsymbol{i_s}}{dt} \right), \tag{3}$$

and

$$\boldsymbol{e_m} = L'_m \frac{d\boldsymbol{i_m}}{dt} = L'_m \left(\boldsymbol{\omega_r} \otimes \boldsymbol{i_m} - \frac{1}{T_r}\boldsymbol{i_m} + \frac{1}{T_r}\boldsymbol{i_s} \right). \tag{4}$$

We use the back EMF vector, $\boldsymbol{e}_m$, instead of the rotor flux vector that was used in the previous model-reference adaptive system (MRAS) schemes [1, 2] for speed identification. A new MRAS system is obtained as shown in Fig. 1. In Fig. 1, the rotor speed estimate, $\hat{\boldsymbol{\omega}}_r$, is produced by the adaptation mechanism expressed as follows:

$$\hat{\boldsymbol{\omega}}_r = \left(K_P + \frac{K_I}{p.} \right) \left(\hat{\boldsymbol{e}}_m \otimes \boldsymbol{e_m} \right), \tag{5}$$

where *p.=d/dt*, $\hat{\boldsymbol{e}}_m$ is calculated from Equation (4) and estimated rotor speed $\hat{\boldsymbol{\omega}}_r$, and K_P and K_I are the adaptation gains. The inductance L'_m can be conveniently incorporated into the adaptation gain constants K_P and K_I in Equation (5). Fig. 2 shows the block diagram of the back EMF-based speed estimation system. It is noticeable that the adaptation mechanism is a vector follower, which guarantees the orientation of the vector regardless of the magnitude. Therefore, the inductance, L'_m, has no influence in the estimation as long as the adaptation gains are high enough. Accordingly, L'_m is not needed and not included in Fig. 2.

The system configuration of the vector control using the back EMF speed identification for electric bus is shown in Fig. 3. It has been shown that the adaptation mechanism expressed in Equation (5) guarantees the stability of the system [3]. The proportional and integral gains, K_P and K_I, can be chosen as high as possible. The only limitation is noise consideration.

In Fig. 3, I^*_m is the magnetizing current reference and I'_r is the torque current command. A first-order low-pass filter (LPF) is needed to filter out switching ripples in the motor voltage and current before being sent to the estimator. The control system including the estimator is based on a digital signal processor (DSP) controller.

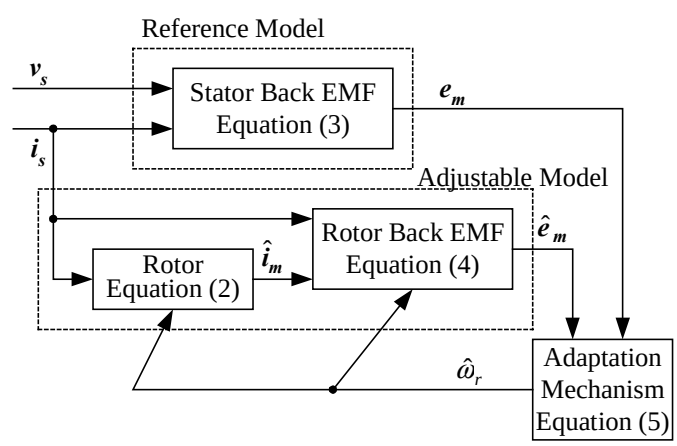

Fig. 1. Structure of back EMF based MRAS for speed identification.

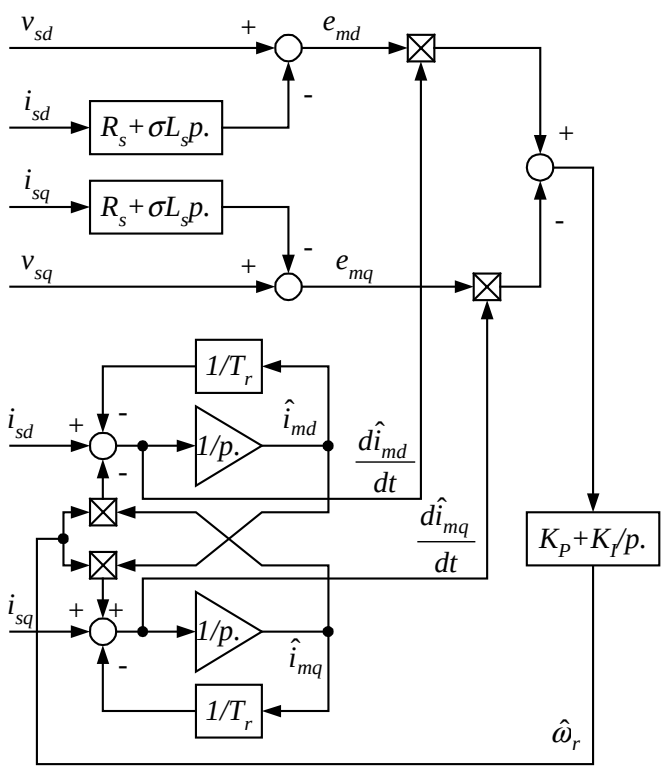

Fig. 2. Block diagram of the back EMF speed estimator.

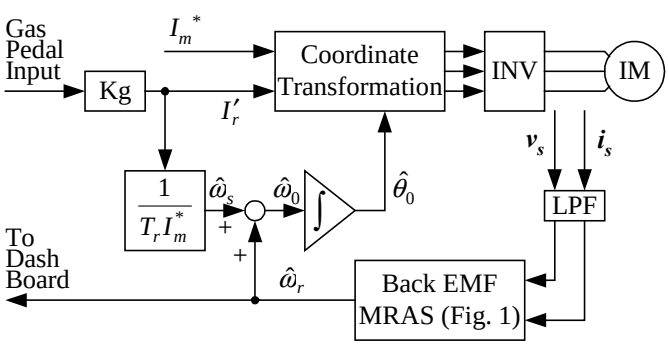

Fig. 3. System configuration of vector control using the back EMF MRAS.

PARAMETER SENSITIVITY OF SPEED ESTIMATION

It is obvious that the speed estimation is dependent on the motor model and parameters. From Fig. 2 and Equations (1) ~ (5), one can see that the speed estimation accuracy is sensitive to the following motor parameters: R_S, σL_S, and T_r. Among them, the inductance, σL_S, does not vary with temperature but is influenced by the magnetizing current level. They can be tuned precisely. However, the resistance R_S and rotor time constant T_r are temperature-dependent and may change in a 1:2 ratio over the motor operation range. This temperature variation of the stator and rotor resistance affects the estimation accuracy. One remedy is to correct the resistance values according to the motor temperature, since temperature sensors are usually present in electric vehicle applications.

As an example, the parameter sensitivity can be analyzed in the following manner. Considering that the value of the stator resistance has some error (ΔR_s), Equation (3) becomes

$$\boldsymbol{e_m} = \boldsymbol{v_s} - \left((R_s + \Delta R_s)\boldsymbol{i_s} + \sigma L_s \frac{d\boldsymbol{i_s}}{dt} \right). \tag{6}$$

If the MRAS successfully maintains nearly zero error, the adjustable model tracks the reference model so that

$$\begin{aligned} &\boldsymbol{v_s} - \left((R_s + \Delta R_s)\boldsymbol{i_s} + \sigma L_s \frac{d\boldsymbol{i_s}}{dt} \right) \\ &= L_m' \left([\boldsymbol{\omega_r} + \Delta\boldsymbol{\omega_r}(R_s)] \otimes \boldsymbol{i_m} - \frac{1}{T_r}\boldsymbol{i_m} + \frac{1}{T_r}\boldsymbol{i_s} \right) \end{aligned} \tag{7}$$

where (ΔR_s), is the stator resistance error and $\Delta\omega_r(R_s)$ is the resultant error in the rotor speed. From Equation (7), the resultant speed error can be approximately expressed as

$$\Delta\omega_r(R_s) = \frac{I_s}{I_m L_m'} \Delta R_s = \frac{1}{L_m'} \sqrt{1 + \left(\frac{I_r'}{I_m} \right)^2} \Delta R_s \tag{8}$$

where I_s is the amplitude of the stator current and I_r' is the torque current. Fig. 4 shows the curves of the rotor speed error versus stator resistance error under 0%, 50%, and 100% of the rated torque. Similarly, speed error from the leakage inductance can be analyzed.

Again, if the adjustable model tracks the reference model and the same value of Tr is used in the MRAS adjustable model and in the function block of Fig. 3 for slip frequency calculation, then we have the following relations:

$$\omega_0 = \hat{\omega}_0 \quad \text{and} \quad T_r \omega_s = (T_r + \Delta T_r)\hat{\omega}_s \tag{9}$$

Therefore, the speed error resulting from the rotor time constant's error is shown as follows:

$$\Delta\omega_r(T_r) = \left(1 - \frac{T_r}{T_r + \Delta T_r} \right) \frac{I_r'}{T_r I_m} = \frac{\Delta T_r}{T_r + \Delta T_r} \cdot \frac{I_r'}{T_r I_m} \tag{10}$$

Fig. 5 shows the curves of the rotor speed error in percentage based on the maximum 100 km per hour (or 60 miles per hour, MPH) speed or 240 Hz rotor speed. A 5% speed error means a 3 MPH vehicle speed or 12 Hz rotor speed error, which is significant at zero or near zero speeds.

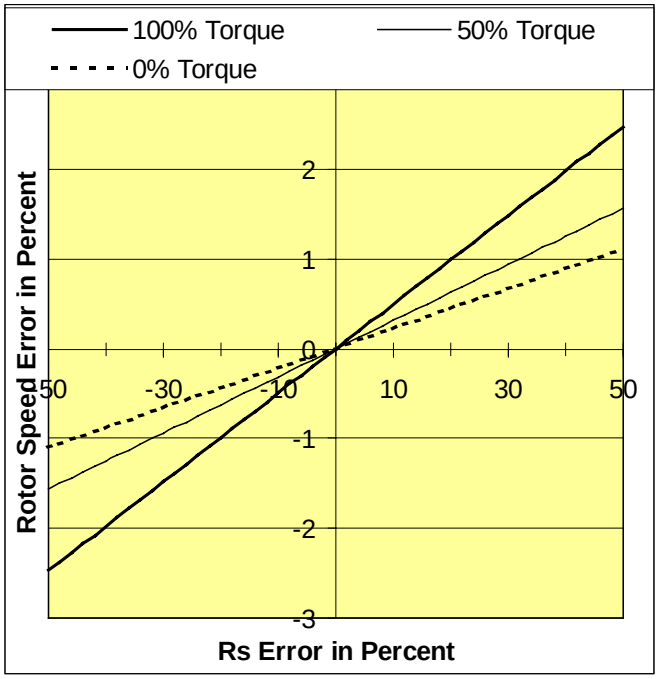

Fig. 4. Speed error due to stator resistance error.

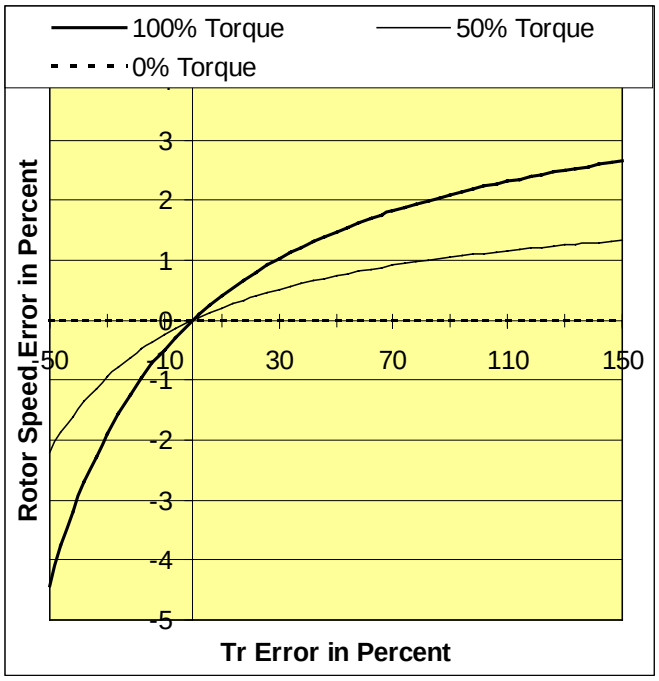

Fig. 5. Speed error due to rotor time constant error.

DSP CONTROLLER, INVERTER, MOTOR, AND BUS SYSTEM

Fig. 6 shows the 100 kW soft-switching inverter and bus photos. As can be seen from the photo, the inverter is very compact and light. The key figures (power density) achieved are: 5kW/kg and 9kW/liter. The inverter is liquid-cooled and rated at 300A (rms) continuous, 600A peak, and 400V DC link. The switching frequency is 10 kHz. The induction motor can generate 200 N·m torque at the 300 A (rms) rated current. The rated maximum motor speed is 15,000 rpm, which yields 100 km per hour or 60 MPH. The bus is 6.7 m (22 feet) long with 10 tons of body weight. The speed sensorless control is implemented on a TI TMS320F240 DSP controller. Only the motor current and DC link voltage are sensed and fed into the controller. The motor voltage or inverter output voltage is calculated from the DC link voltage and space vector PWM pattern. The dead time (equivalent dead time from soft switching) compensation is added to the PWM pattern to generate gate signals. This voltage calculation shows sufficient accuracy at speeds beyond 3 MPH. However, at lower speed a direct voltage sensing as shown in Fig. 3 becomes necessary when a more accurate speed estimation is required.

Fig. 6. Photos of the 100 kW soft-switching inverter and electric bus.

ROAD TEST

Extensive road testing has been performed. The back EMF based MRAS system provided a very smooth start, and good torque control at low speeds. The results are satisfactory. Fig. 7 shows start-up and acceleration

waveforms calculated from the equivalent road testing. At start-up, a relatively large breakaway torque is required, which is followed by a steady acceleration to 20 MPH (or 32 kilometer per hour) in 15 seconds. After the vehicle reaches the desired speed, the torque is reduced to match the road load. A smooth acceleration is observed. In the bus control system, the acceleration (gas) pedal is used to command acceleration (motoring) and deceleration (regen) torque as illustrated in Fig. 8. The first 20% of the pedal position is used for regenerative (braking) torque control. The zero-torque command point is at about 20% of the total accelerator pedal travel, and when the torque command is negative (i.e., accelerator pedal position between 0-20%), a corresponding amount of regenerative braking torque is commanded. The bus operator perceives an effect similar to "engine braking" in an engine-powered vehicle. When the mechanical brake is pressed, the regen torque increases with a time constant of 1 sec from 50% (the value when the accelerator pedal is all the way up) to 100% regen torque. Further brake pedal travel maintains 100% regen torque and progressively activates the conventional friction brakes until 100% of the total braking force available is being produced. Therefore, mechanic braking is minimized while the regen braking is maximized. Fig. 9 shows the bus test cycle used in the road testing, which shows the typical driving cycle to maximize regeneration. Fig. 10 shows inverter and motor waveforms during vehicle acceleration, where V_b is the quasi-resonant DC link voltage of the soft-switching inverter, I_r is the resonant current for soft-switching and I_{motor} is the motor current.

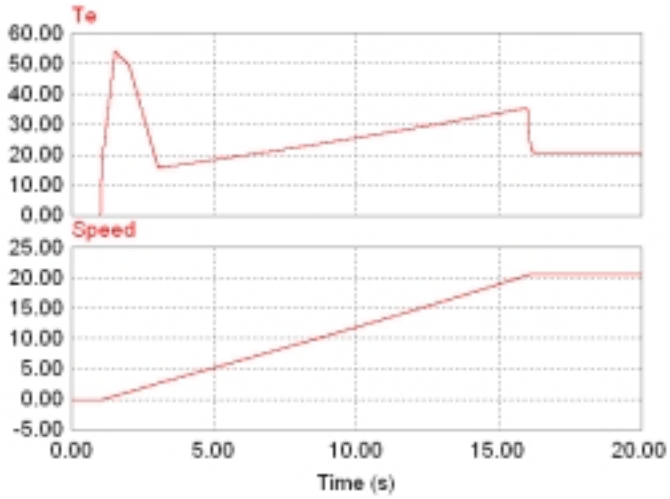

Fig. 7. Calculated road test results of acceleration 20 MPH in 15 seconds. Top trace: motor torque (N m), bottom trace: bus speed (MPH).

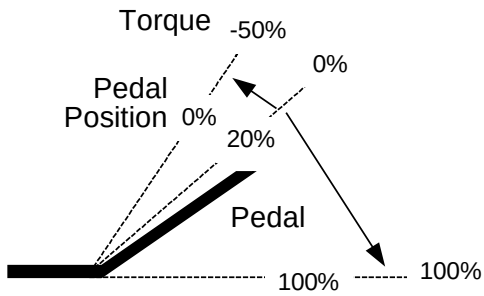

Fig. 8. Using gas pedal for motoring and regen torque command.

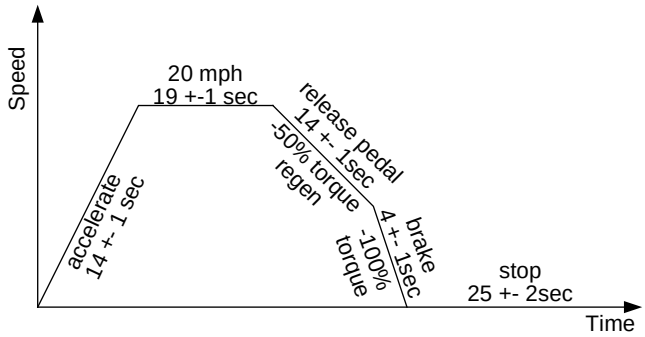

Fig. 9. Bus test cycle.

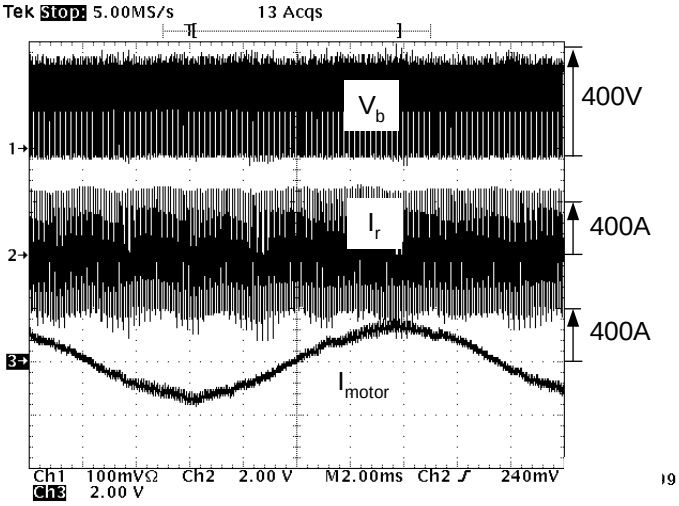

Fig. 10. Inverter and motor waveforms.

CONCLUSION

This paper presented a speed- and flux-sensorless induction motor drive system implemented with a new 100 kW soft-switching inverter and DSP control for electric vehicle applications. The speed identification method is based on the motor back EMF information that can be obtained indirectly from the motor voltage and current. Compared with the traditional flux observer methods, the back EMF based MRAS does not require pure integral operation that is difficult to implement at low and zero speeds, thus improving performance and reducing complexity of implementation. Test results showed satisfactory performance for electric vehicle applications.

ACKNOWLEDGMENTS

The authors would like to thank many others involved in this project, especially our Oak Ridge National Laboratory colleagues for their contributions and Advanced Vehicle Systems, Inc /CARTA for their support in road testing.

CONTACTS

Fang Z. Peng and Donald J. Adams
Oak Ridge National Laboratory
P.O. Box 2009, Bldg. 9102-1, MS 8038
Oak Ridge, Tennessee 37831-8038
Phone: 865-576-7261; 576-0260, Fax: 865-241-6124,
Email: pengfz@ornl.gov, ajd@ornl.gov.

REFERENCES

[1]. C. Schauder, “Adaptive speed identification for vector control of induction motors without rotational transducers,” IEEE/IAS Annual Meeting 1989, pp. 493-499.

[2]. S. Tamai et al., “Speed sensorless vector control of induction motor with model reference adaptive system,” IEEE/IAS Annual Meeting 1987, pp. 189-195.

[3]. F. Z. Peng and T. Fukao, “Robust speed identification for speed-sensorless vector control of induction motors,” *IEEE Transactions on Industry Applications*, Vol. 30, No. 5, pp. 1234–1240. Sept./Oct. 1994.

[4]. M. Beck and D. Nuanin, “A new method for the calculation of the slip frequency for a sensorless speed control of a squirrel-cage induction motor,” IEEE/PESC 1985, pp. 678-683.

[5]. A. Abbondanti and M. Brenne, “Variable speed induction motor drives use electronic slip calculator based on motor voltages and currents,” IEEE Trans. Ind. Appl., vol. 11, no. 5, pp. 483-488, 1975.

[6]. A. Fratta et al., “Vector control of induction motors without shaft transducer,” IEEE/PESC, 1988, pp. 829-492.

[7]. K. Hurst, T. Habetler, G. Griva, and F. Profumo, “Zero-speed tacoless IM torque control: simply a matter of stator voltage integration,” IEEE Trans. Ind. Appl., vol. 34, no. 4, pp. 790-795, 1998.

[8]. T. Lipo and K. Chang, “A new approach to flux and torque sensing in induction machines,” IEEE Trans. Ind. Appl., vol. 22, no. 4, pp. 731-737, 1986.